IOP Conference Series: Earth and Environmental Science

PAPER • **OPEN ACCESS**

Parametric Analysis of Urban Flood Risk Based on 'Shallow Water' Model; a Real Case at Small Scale

To cite this article: Antonio Pasculli *et al* 2019 *IOP Conf. Ser.: Earth Environ. Sci.* **362** 012156

View the article online for updates and enhancements.

This content was downloaded from IP address 79.13.18.33 on 15/11/2019 at 12:50

Parametric Analysis of Urban Flood Risk Based on 'Shallow Water' Model; a Real Case at Small Scale

Antonio Pasculli[1], Jacopo Cinosi[1], Alain D'Ettorre[1], Nicola Sciarra[1]

[1] Department of Engineering and Geology (InGeo), University G. D'Annunzio of Chieti-Pescara, Italy

a.pasculli@unich.it

Abstract. In this paper, we examined the increased risk of urban flooding due to incorrect or insufficient maintenance of small hydrological basins. In particular, the effects of a peak rainfall event on a water drainage canal near to a town in central Italy were considered. By means of the RiverFlow2D commercial computational software, the *Shallow water* technique was chosen, which is based on the Finite Volume Element and on the Godunov-Riemann technique. We also experimented with parallel computing, by performing the same calculations with GPUs (Graphics Processing Units) and we were able to significantly reduce the total time by 80 times. The study area is located in Pianello di Ostra district (Ancona, Marche, Italy). The peak rain data, which is publicly available, were recorded by the Corinaldo pluviometric station (9.1 km from the area) between April 26th and May 2nd 2014 and it caused a subsequent flooding event lasting two days. We integrated pluviometric data with available cartography, a rigorous site inspection, interviews with inhabitants and a high-resolution topographic survey (30 x 30 cm) acquired with a drone. To process rainfall data, we selected the Curve-Number (CN) empirical method, developed by the USDA Natural Resources Conservation Service (SCS). The parametric simulations on Fosso della Trocca basin were performed considering both pre-flooding maintenance state, with obstructions of the channel and the presence of a small bridge, and optimal maintenance state, with no obstructions and no bridge. The computer-simulated depth of the flooding water was compatible with what was observed during the real flood. Thus, the effects of increasingly intense rainfall events were estimated. However, we found that threshold values exist above which no ordinary maintenance is sufficient to avoid flooding phenomena.

1. Introduction

The *Computational Fluid Dynamics* (CFD) numerical method, the most advanced approach for studying flow phenomena, is based on the solution of the balance equations of physics and it relies on solving Navier-Stokes [1] equations as well as on experimental laws describing mass transport of material, rate of erosion [2], etc. In order to avoid the cumbersome process of establishing a suitable meshing, a mesh-less solution of the differential equation was also proposed. The *Smoothed Particle Hydrodynamics* (SPH) method appears to be promising ([3], [4], [5], [6], [7]). *Cellular Automata* (CA) model [8] is also a relevant alternative to CFD and it is particularly suited for predicting morphological changes within a

Content from this work may be used under the terms of the Creative Commons Attribution 3.0 licence. Any further distribution of this work must maintain attribution to the author(s) and the title of the work, journal citation and DOI.
Published under licence by IOP Publishing Ltd

large area and over an extended period of time (compatible with climate evolution), both at reach [9], [10] and at catchment scale [11]. Given our study case involving a short time frame, reasonable simplifications of the CFD technique could be applied. The *Shallow water* method implemented in RiverFlow2D [12] was chosen to perform all simulations. These methods have proved to be useful for inspecting morphological variations of a landscape [13], fast Alpine debris flow [14] and Urban floods. RiverFlow2D also allows to account for frequent wetting/drying cycles induced by rainfall variation, which may lower soil mechanical strength (e.g. for pyroclastic soil [15], [16]), thus triggering possible erosion occurrences and morphological variations. Turbulence [17] is omitted by the current version of the code.

2. Mathematical and Numerical modelling

RiverFlow2D is based on the *Surface Water Modeling System* (SMS) Graphical User Interface (GUI). The most realistic approach should aim for 3D modelling, but computational time costs needed for the space and time framework of the case study would have been significantly longer. Therefore, the *Depth-Averaged 2D*, *Shallow water*, approach [18] implemented by the software, which assumes the vertical depth of the flow is negligible compared to the flow's other dimensions, was an appropriate choice. In order to account for bed level jumps (considered as source terms in the related differential equations) found in the morphology of landforms, the software includes the *Augmented approximate Riemann solvers* approach. Moreover, RiverFlow2D allows for parallel computing of numerical computations on the *Graphics Processing Unit* (GPU) hardware, which can have thousands of processors, capable of significantly reducing the total computation time by orders of magnitude: we measured a GPU total time about 80 times shorter than CPU. In the following sub-sections, we'll briefly discuss mathematical and numerical methods used in this work as described by [12], which we refer to for further details.

2.1. Hydrodynamic unsteady flow models

The following system results from combining partial differential equations, based on water volume conservation, water momentum conservation and shallow water assumption [19]

$$\frac{\partial \boldsymbol{F}(\boldsymbol{U})}{\partial t}+\frac{\partial \boldsymbol{F}(\boldsymbol{U})}{\partial x}+\frac{\partial \boldsymbol{G}(\boldsymbol{U})}{\partial t}=\boldsymbol{S}(\boldsymbol{U},x,y) \tag{1}$$

$$\boldsymbol{U}=\left(h,\, q_x,\, q_y\right)^T;\ \boldsymbol{F}=\left(q_x,\, \frac{q_x^2}{h}+\frac{1}{2}gh^2,\, \frac{q_x q_y}{h}\right)^T;\ \boldsymbol{G}=\left(q_y,\, \frac{q_x q_y}{h},\, \frac{q_y^2}{h}+\frac{1}{2}gh^2\right)^T \tag{2}$$

$$\boldsymbol{S}=\left(0,\, \frac{p_{bx}}{\rho}-\frac{\tau_{bx}}{\rho},\, \frac{p_{by}}{\rho}-\frac{\tau_{by}}{\rho}\right)^T \tag{3}$$

where h is the water depth, $q_x = h\mathrm{u}$ and $q_y = h\mathrm{v}$ are the unit discharges resulting from the *shallow water* approach, (u,v) are the x and y depth-averaged components of the velocity vector $\mathbf{u}$, g is the gravity acceleration and $gh^2/2$ is the flux obtained from the assumption of a hydrostatic pressure distribution in every water column, commonly found in *shallow water* models. The source term $\boldsymbol{S}(\boldsymbol{U},x,y)$ integrates the effect of pressure forces, p_{bx} and p_{by}, over the bed and the tangential forces, τ_{bx} and τ_{by}, generated by the bed stress. Note that $p_{bx}/\rho = ghS_{0x}$ and $p_{by}/\rho = ghS_{0y}$, while $S_{0x} = -\partial z/\partial x$ and $S_{0y} = -\partial z/\partial y$ are the bed slopes of the bottom level z. The rheological laws used to calculate the tangential forces τ_{bx} and τ_{by} assumed a *Clear-water* option, based on the Manning friction law

$$\tau_{bx} = S_{fx} \equiv \frac{n^2 \mathrm{u}\sqrt{\mathrm{u}^2+\mathrm{v}^2}}{h^{4/3}};\qquad \tau_{by} = S_{fy} \equiv \frac{n^2 \mathrm{v}\sqrt{\mathrm{u}^2+\mathrm{v}^2}}{h^{4/3}} \tag{4}$$

where n is the Manning's roughness coefficient, related to flow in water channels.

2.2. Manning's coefficient

The Manning's *n* coefficient usually accounts for the effects of the bed roughness, internal friction and variations in shape and size of the water channel or canal cross-section, as well as for the effects of obstructions and river meandering. This kind of coefficient was partially used to fine-tune parameters during the calibration process, in order to adjust the numerical results compared to measured data. The initial estimated parameters for this paper were based on the tables reported in [20]. The software allows to consider a variable Manning's coefficient within the studied basin, by the means of appropriate polygonization, proportional to the flow depth.

2.3. Numerical solver

The general numerical approach used in this work is based on the Finite-volume scheme, which proceeds with an integration on a volume expressed as a grid-cell Ω, using Gauss theorem

$$\frac{\partial}{\partial t}\int_{\Omega} \boldsymbol{U} d\Omega + \oint_{\partial\Omega} \boldsymbol{E}(\boldsymbol{F},\boldsymbol{G})\cdot \boldsymbol{n} ds = \int_{\Omega} \boldsymbol{S} d\Omega \tag{5}$$

Where $\boldsymbol{U}$, $\boldsymbol{F}$, $\boldsymbol{G}$ and $\boldsymbol{S}$ are the vectors already described in (2), $\partial\Omega$ is the volume domain boundary, $\boldsymbol{n}(n_x, n_y)$ is the outward unit normal vector to the volume Ω. Then, a piecewise representation of the conserved variables and an upwind and unified formulation of fluxes and source terms is applied [18]:

$$\frac{\partial}{\partial t}\int_{\Omega_i} \boldsymbol{U} d\Omega + \sum_{k=1}^{(\text{Number of Edges})_i} (\boldsymbol{E}\cdot\boldsymbol{n} - \bar{\boldsymbol{S}})_k A_k = 0 \tag{6}$$

Where Ω_i is the volume of the i-th computational cell, whose area of the k-th edge face is A_k. Finally, the approximate solution is calculated as a sum of jumps or shocks, also involving rarefactions.

2.4 Optimal time-step computation

Identifying an optimal time-step is paramount to assess appropriate parameters, in order to obtain computational stability of chosen algorithms. RiverFlow2D implements an automatic procedure for this, based on the solution of the so-called *Riemann Problem* (RP) [18]. In 1D simulations, the time-step is chosen small enough to avoid the interaction of 'numerical waves', emerging from the application of this approach, and the 'equivalent distance' $\Delta x/2$ between neighbour mesh cells is introduced. On the other hand, when working with 2D simulations with unstructured meshes, the equivalent distance (referred to as L_i) must consider the 'volume' of the cell and the length of the shared edges:

$$L_i = \frac{A_i}{\max\limits_{k=1,\ NE} l_k} \tag{7}$$

Where A_i is the 'volume' (area in 2D) of the *i-th* cell, l_k is the length of the *k-th* edge of the *i-th* cell. Considering that each *k-th* RP (along the direction perpendicular to the *k-th* edge) is used to deliver information to a pair of neighbour cells of different sizes, the associated distance between *i-th* and *j-th* cell $\min(L_i, L_j)/l_k$ results to be relevant. Furthermore, in the case of triangular cells the procedure based on RP requires that the time-step size is limited by

$$\Delta t \le CFL \cdot \frac{\min(L_i, L_k)}{\max\limits_{m=1,2,3} \left|\tilde{\lambda}_m\right|} \tag{8}$$

Where *CFL* is the *Courant-Friedrichs-Lewy* number (for 1D case $CFL=(u\cdot\Delta t)/\Delta x$, with u as the flow velocity, Δt as the investigated *time-step* and Δx as the *mesh-size*) and $\tilde{\lambda}_m$ is the velocity of the flow perpendicular to the *m-th* edge, resulting from the application of the 1D RP solver along the three directions in the case of triangular cells. The CFL number has to be defined by the user and a value of *CFL* = 1 was assumed for all simulations.

3. Test case

The studied area is located on the relatively flat surface of a fluvial terrace, close to the edge of the hill scarps and slopes that delimit the valley of Misa river, along the Trocca Canal, a left tributary of Misa river. Outcrops surfacing in the area are mostly attributed to alluvial fan deposits, consisting of continental quaternary covers forming the distinctive slightly convex fan shape, resulting from the fluvial transport and later deposition of mostly fine sediments. The lithology consists mostly of clays and silts with locally embedded sandy lenses, covering gravels composed predominantly by limestone clasts, laying on top of the clay-marly plio-pleistocene bedrock. Hydrography and orography are primarily characterized by the Trocca Canal, a water channel with an almost rectangular cross-section, running at the center of its valley in a basin extending for about 2 km^2. Altitude ranges from 50 m a.s.l. to 173 m a.s.l. and several erosional scarps broadly affected by vegetation (arboreal and shrubby associations) shape hill slopes on the sides of the valley. Vegetation tends to restrain the water flow, thus resulting in a limiting effect on water runoff. Just upstream of Pianello di Ostra, the canal is crossed by a street junction between two roads (S.P. 360 and S.P. 360/01 variant) and then proceeds as an open-air section throughout the town of Pianello di Ostra, down to the road S.P. Arceviese, where water then flows into a 135 m-long culvert, crossing the road and part of the town. The final section of the canal runs as open air again, contained by concrete walls on the sides and bottom, up to the confluence with Misa river. As said, the general hydrogeological scheme is represented by silty clays with thin sand intercalations on top and by gravels with a sand matrix on the bottom. The clayey lithotypes has a medium-low permeability, but sand intercalations can locally and sharply increase permeability allowing for discontinuous water levels, while the gravel lithotype on the bottom has the highest permeability, allowing water to flow through it.

4. Simulations

The following assumptions were made in order to perform parametric simulations

1. The Curve Number (CN) method was adopted [21];
2. The rainfall input was constant over time (needed for the application of the CN method to estimate the amount of runoff water);
3. All runoff water from the upstream basin flowed into the canal we're investigating;
4. No evaporation nor infiltration phenomena occurred, except for what was already accounted for by the CN method;
5. The Pezzoli's law was used to estimate the time of concentration (required by the CN method);
6. The rainfall curve was provided by the regional weather-hydro-pluviometric information system SIRMIP website (http://app.protezionecivile.marche.it/sol/);
   About rainfall parameters:
7. Once the CN method was applied, the value of the Antecedent Moisture Conditions (AMC) was calculated;
8. The rainfall data of the 5 days preceding the flooding event were considered, in order to assess the total volume of water available for runoff
9. There are effects subtracting water from the runoff, such as soil saturation and trapping of water in morphological depressions;
10. The higher the CN, the higher the total volume of water available for runoff.

Figure 1 shows the available rainfall data and its cumulate curve of the 5 days preceding the flooding event, recorded by pluviometric station of Corinaldo (Ancona, Marche, Italy). The peak data refers to May 2nd, 2014 (~160 hours from 26th April 2014 13:00 GMT+2).

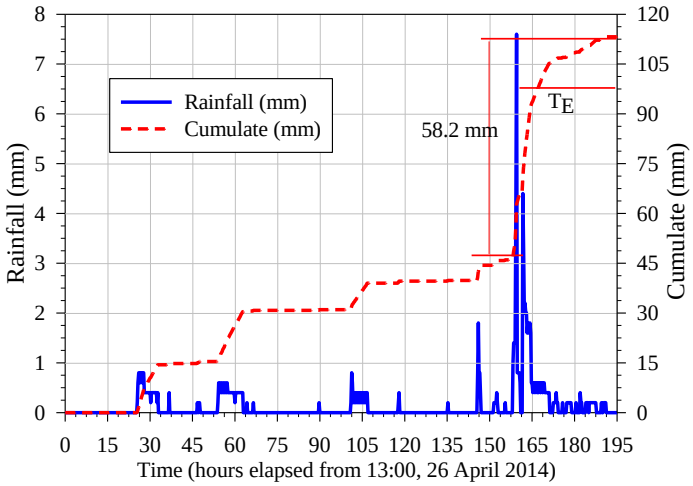

Figure 1. Rainfall and Cumulate diagram of the flooding event, measured by the pluviometric station in Corinaldo (Ancona, Marche, Italy).

4.1. Curve Number Method (CN)

The Curve Number (CN) method, developed by USDA Natural Resources Conservation Service (SCS) [21], is an empirical method based on rainfall and runoff measurements performed on small river basins. The process has proven to be very effective for estimating the total amount of runoff, given an area and rainfall input data. An input pluviometry inflow $P[mm]$ does not generate outflow until its value reaches a threshold called Absorption Capacity $I_a[mm]$, since a part of the inflow infiltrates through the soil or is retained by morphological depressions. The specific surface runoff $Q_p[mm]$ is proportional to the rainfall inflow as the the specific infiltrated volume $F[mm]$ is proportional to the maximum potential retention of the soil $S[mm]$, so that

$$\frac{Q_p}{P - I_a} = \frac{F}{S} \tag{9}$$

Assuming the mass balance condition $F = P - I_a - Q_p$, it follows that

$$Q_p = \frac{(P - I_a)^2}{P - I_a + S} \tag{10}$$

Which estimates the specific runoff volume Q_p as a function of rainfall inflow P and of two parameters I_a and S, specific to each basin. The I_a parameter depends on soil conditions such as initial humidity, retention in morphological depressions, infiltration and land use, therefore it is difficult to quantify it directly. However, an indirect empirical relation ties I_a to S via I_a=0.2 S, from which it follows that

$$Q_p = \frac{(P - 0.2S)^2}{P + 0.8S} \tag{11}$$

Where S can be expressed as a function of the Runoff Curve Number CN, varying from 0 to 100

$$S = 25.4\left(\frac{1000}{CN} - 10\right) \tag{12}$$

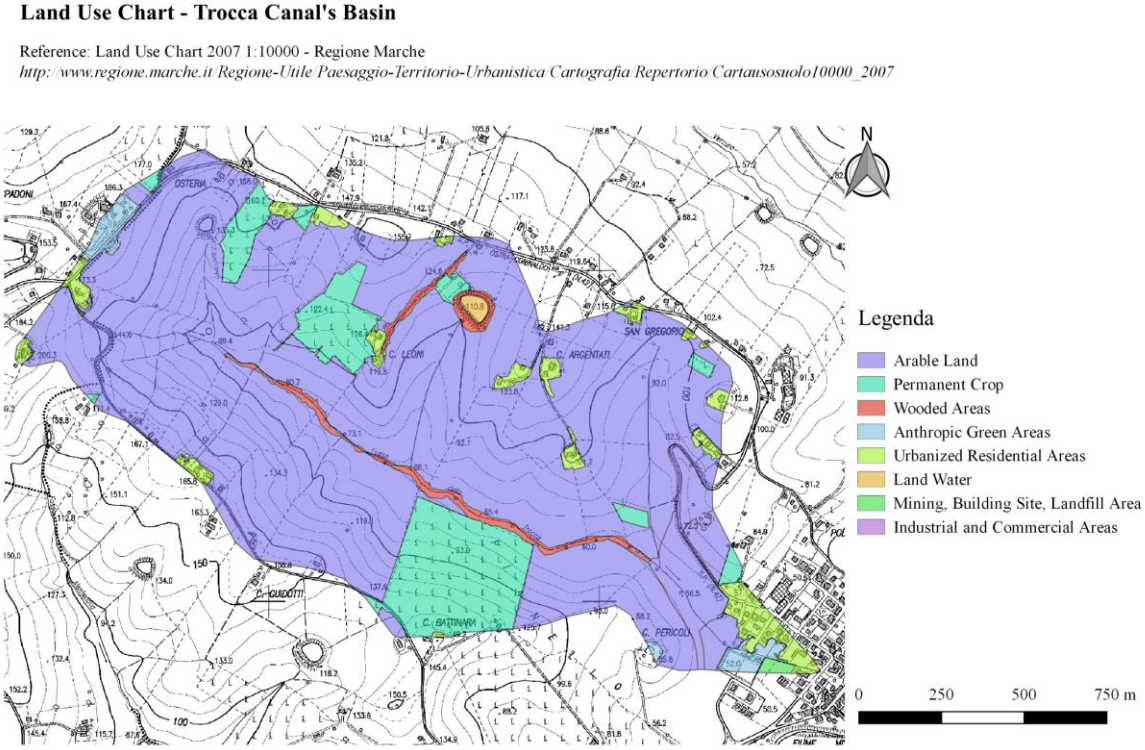

Figure 2. Land Use Chart used for assessing CN coefficients (after [22])

It's worth mentioning that relation (11) has physical meaning only if $P>0.2S$, according to the concept of threshold values discussed earlier. Application of relations (11) and (12) provided us with a set of resulting curves. Each curve has a characteristic CN value (Fig. 3). The CN values are estimated by comparison with specific tables created by the SCS, which account for the grain size and permeability of the soil, for the humidity conditions during the 5 days preceding the flooding event and for the use of the soil. With the help of the Geological Map of the Marche region, scale 1:10,000 (Fig. 2), and by observing the study area on site, we were able to evaluate the average granulometry of the surface deposits and we also determine that most of it (about 92% in Figure 2) had an agricultural land use. Accordingly, the Category C of USDA table was chosen, which is described as a moderately high outflow potential, made up of thin soils and soils containing considerable amounts of clays, soils poor in organic content; poor infiltration and saturation capacity. From Figure 1, a cumulate rainfall of 30 mm was estimated (45 mm at the start of the flooding event minus 15 mm measured 120 hours before the event). Given the event took place during vegetative season, the resulting USDA category according to Table 1 was found to be *Category I*. Consequently, comparing runoff curve numbers for cultivated agricultural lands (freely adopted from [21]) to Table 2, we categorized the soil to be *Soil Group C*. Then, after averaging the values (in bold) of column C from Table 2, CN_I=85 was roughly calculated. However, this CN value results to be valid for *Category II* of the humidity tables ([21], not reported). Hence, the obtained CN_I should be corrected by equations (13) [21]:

$$CN_{II} = \frac{CN_I}{2.38 - 0.0138 \cdot CN_I} \tag{13}$$

From which a new value of CN_{II}=70 could be calculated, which is also valid for the *Category* I of humidity. CN_{II} then substituted CN_I in equation (10) and the corrected value of Q_P describing the *net runoff* of the area could be finally calculated. The following equation gives the maximum flow *Q*

$$Q = \frac{Q_P \cdot A}{t_c} \cdot \frac{1000}{3600} \tag{14}$$

Where A[km^2] is the basin area and $t_c[h]$ is the basin time of concentration, equal to 1.09 h, calculated using Pezzoli's law. The resulting flow curve is a trapezoid, with an ascendant branch having a duration equal to the time of concentration t_c and a descendent branch having a duration equal to 5/3 of t_c. Figure 4 shows two hyetographs: the first (a) considers the maximum flow equal to 4.66 m^3/s, as obtained thorough the previous discussion, while the second (b) considers the maximum flow equal to 13.14 m^3/s (b), assuming Category II in Table 1, needed to perform parametric analysis. The sections at constant flow, reported in Figure 4, were determined assuming that a total of approximately 58.2 mm of rain was experienced within the entire 2 km^2 basin's area, during the time interval T_E shown in Figure 1. Then, after having selected the maximum peak (4.66 mm/s and 13.14 mm/s, Figure 4) and having imposed the numerical equality between the area of the trapezoid (considering abscissas in seconds) and the total volume of rainwater (about 116 m^3) the interval time characterized by constant flow resulted accordingly.

Table 1. Antecedent Moisture Condition (A.M.C.) (freely adapted from [21])

A.M.C. Category	Precipitation height in the previous 5 days (mm)		Description
	Non-vegetative season	Vegetative season	
I	< 12.7	< 35.6	**Minimum runoff potential** The soil is sufficiently dry to allow satisfactory plowing or cultivation
II	12.7 – 27.9	35.6 – 53.3	**Average condition**
III	>27.9	>53.3	**Minimum runoff potential** The soil has been saturated with previous rains

Table 2. Runoff curve numbers for cultivated agricultural lands (freely adapted from [21])

Land use		Treatment or practice	Hydrological condition		Curve numbers for hydrologic *Soil Group*	
			A	B	C	D
Fallow	Straight row	-	77	86	**91**	94
Row crops	Straight row	Poor	72	81	**88**	91
		Good	67	78	**85**	89
	Contoured	Poor	70	79	**84**	88
		Good	65	75	**82**	86
	Contoured and terraced	Poor	66	74	**80**	82
		Good	62	71	**78**	81
Small Grain	Straight row	Poor	65	76	**84**	88
		Good	63	75	**83**	87

5. Conceptual model

Figure 5 illustrates the topographical plot of the spatial domain for the study area. In particular, the cross-section A-A' indicated in the figure is taken perpendicular to the water flow, as if looking at the upstream direction of the canal. Locations for the small bridge (labelled "1") and the culvert (labelled "2") are also given. Figure 6 shows the Manning's coefficient distribution, by means of tables reported in [20]. Figure 7 provides estimates for the velocity of the flow through the culvert, by applying Chezy's law.

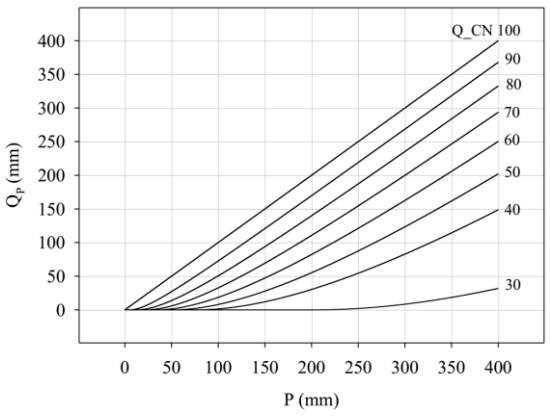

Figure 3. Trend of specific surface runoff as a function of rainfall for different CN values

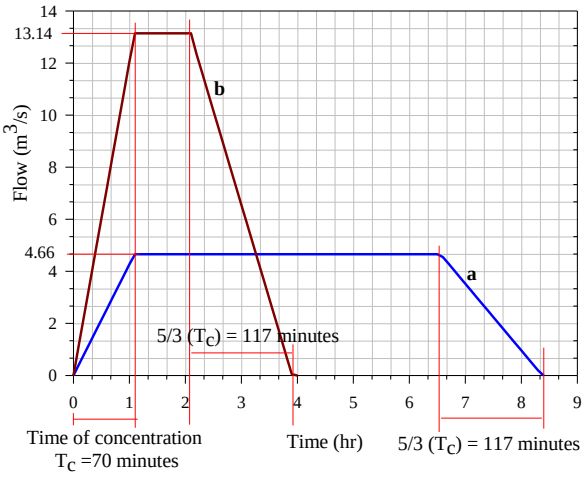

Figure 4. Hyetographs for two different maximum flow rates of 4.66 m^3/s and 13.14 m^3/s

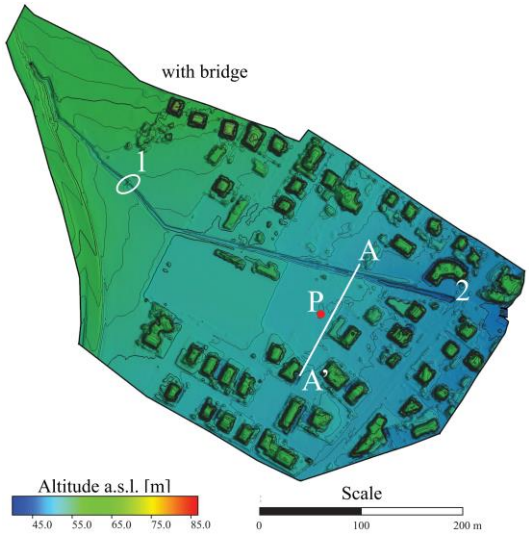

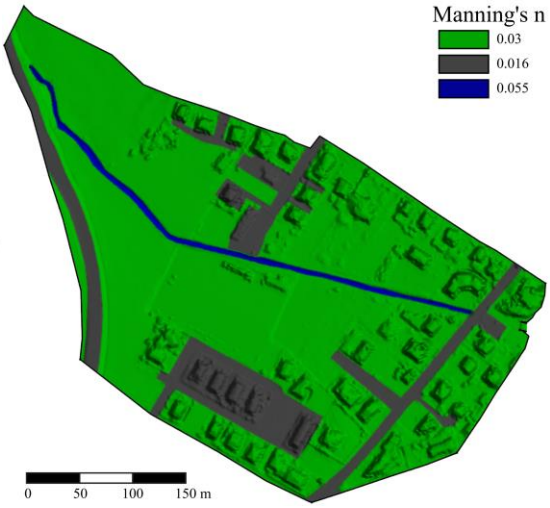

Figure 5. Topographical plots of the spatial domain coefficient selected for the simulations

Figure 6. Distribution of the Manning

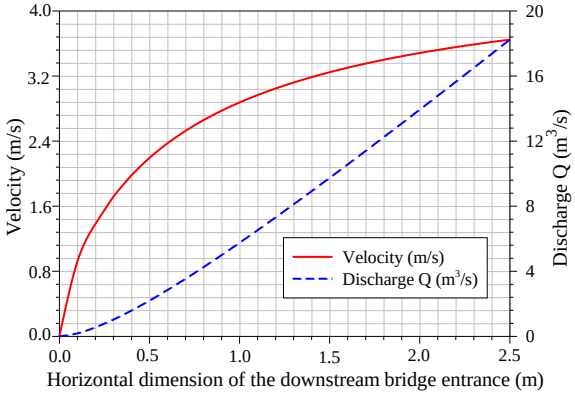

Figure 7. Application of the Chezy formula for calculating the flow rate at the entry of the underpass, indicated with the label 2 in Figure 5

6. Results

Figures 8a-d illustrate the results of performed simulations, which assumed 4.7 m^3/s discharge. In Figure 8a the numerical simulation of what probably happened during the flooding event of May 2014 is shown, while Figure 8b shows the simulation of what would have happened if the channel had been properly maintained, without the presence of the small bridge. Figures 8c and d show water elevation profiles in real and ideal conditions respectively, calculated for cross-section A-A' after 6:30 h from the flooding event. Real conditions (referred as "not clean channel" in figures) means sub-optimal maintenance state of the channel and the presence of the bridge while ideal conditions (referred as "clean channel") include an optimal maintenance state and the absence of the bridge. Figure 9a shows the morphology of the cross-section A-A' of the channel in both "clean" and "not clean" states.

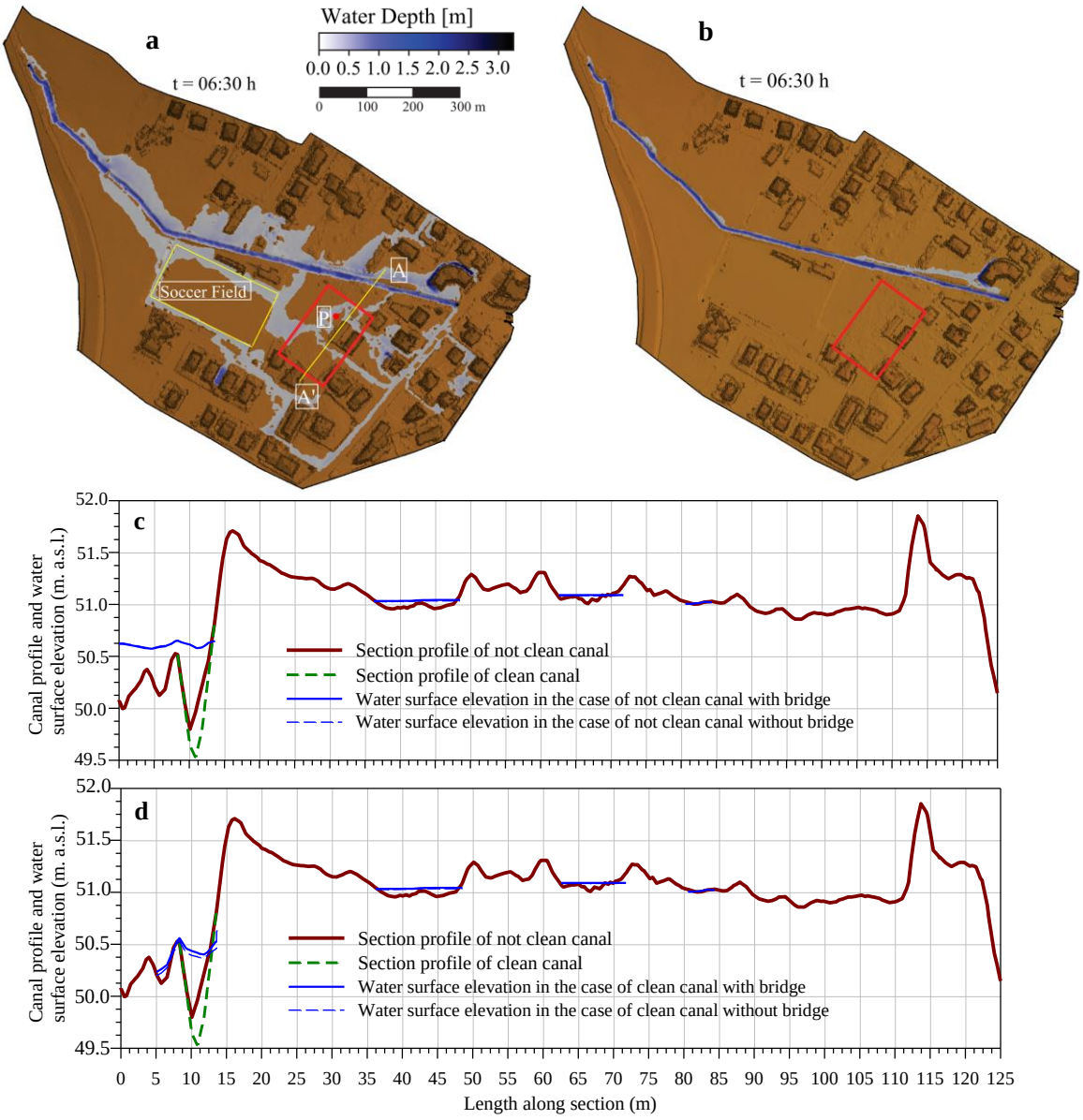

Figure 8. 4.7 m^3/s water discharge is assumed; a) not clean canal with small bridge; b) clean canal without small bridge; c) not clean canal, profile of water surface elevation, with small bridge; d) clean canal, profile of water surface elevation with and without small bridge (freely adapted from [22])

As these figures highlight, the calculated simulations were found to be quite consistent and significantly adherent to the available data for the flooding event examined. Also, resulting simulated values of about 50 cm of water depth (specifically along the A-A' cross-section) are mainly compatible with experimental values both collected from observations of inhabitants and pictures taken immediately after the flooding. It's worth noticing that the soil of the soccer field (indicated in Figure 8a) rose about 30 cm during the flooding event, which completely invaded the field. This calculation was made possible by recent topographic data and simulations clearly show this uplifting effect as well.

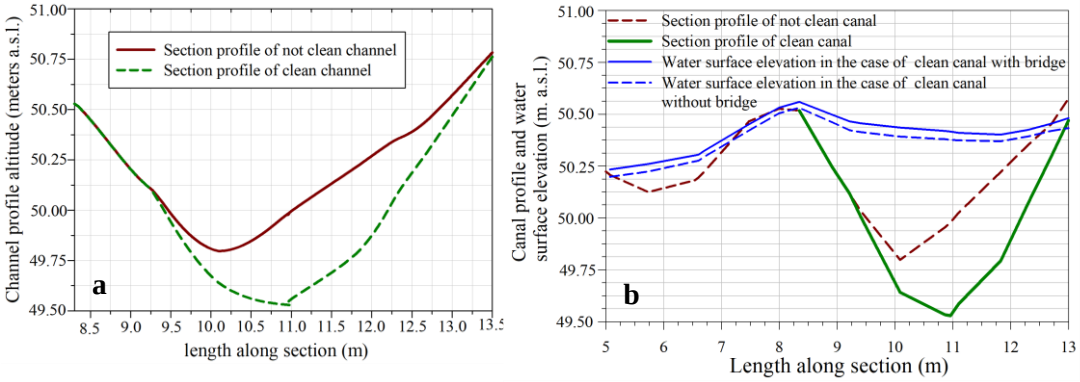

Figure 9 a) the A-A' cross-sections (in Figure 3) of clean and not clean channel; **b**) 4.7 m^3/s discharge, clean canal with and without without bridge after 6:30 h since the selected start of the event (after [22])

Figure 9b illustrates a zoomed portion of the cross-section shown in Figure 8d, while Figure 10 shows the variation of the water elevation at point P indicated in Figure 8a. It is clear that the presence of the small bridge has a noticeable effect, even from a certain distance.

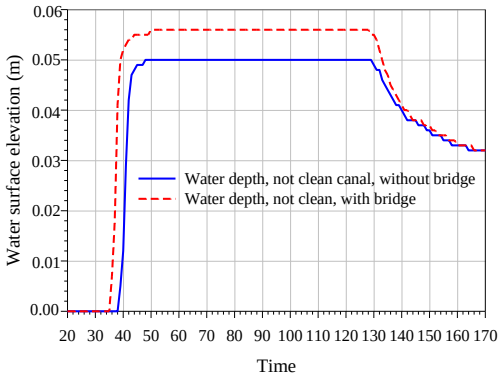

Figure 10 Water elevation profile over time, calculated at point P (Figures 5 and 8a); 4.7 m^3/s discharge, not-clean canal with bridge after 6:30 h since the selected start of the event

Figure 11 shows an overview of the maximum flood levels for different values of the maximum flow rate, as defined earlier in this paper. Lastly, Figure 12 shows the estimated risk maps for adult individuals, resulting from the procedure described in [23], with higher risks represented by higher numerical indices. The labels C, D, YB and NB mean, respectively, Clean, Dirty, Yes-Bridge and No-Bridge.

7. Conclusion

The application of numerical modelling techniques, such as the *Shallow water* method used in this paper, coupled with a high-resolution topographical model, has proven to be a powerful tool for predicting the response of the surface water drainage system to a reference rainfall event. Furthermore, the procedure proposed by the United States Department of Agriculture was very effective in determining the reference flow rate, on which further parametric calculations were developed.

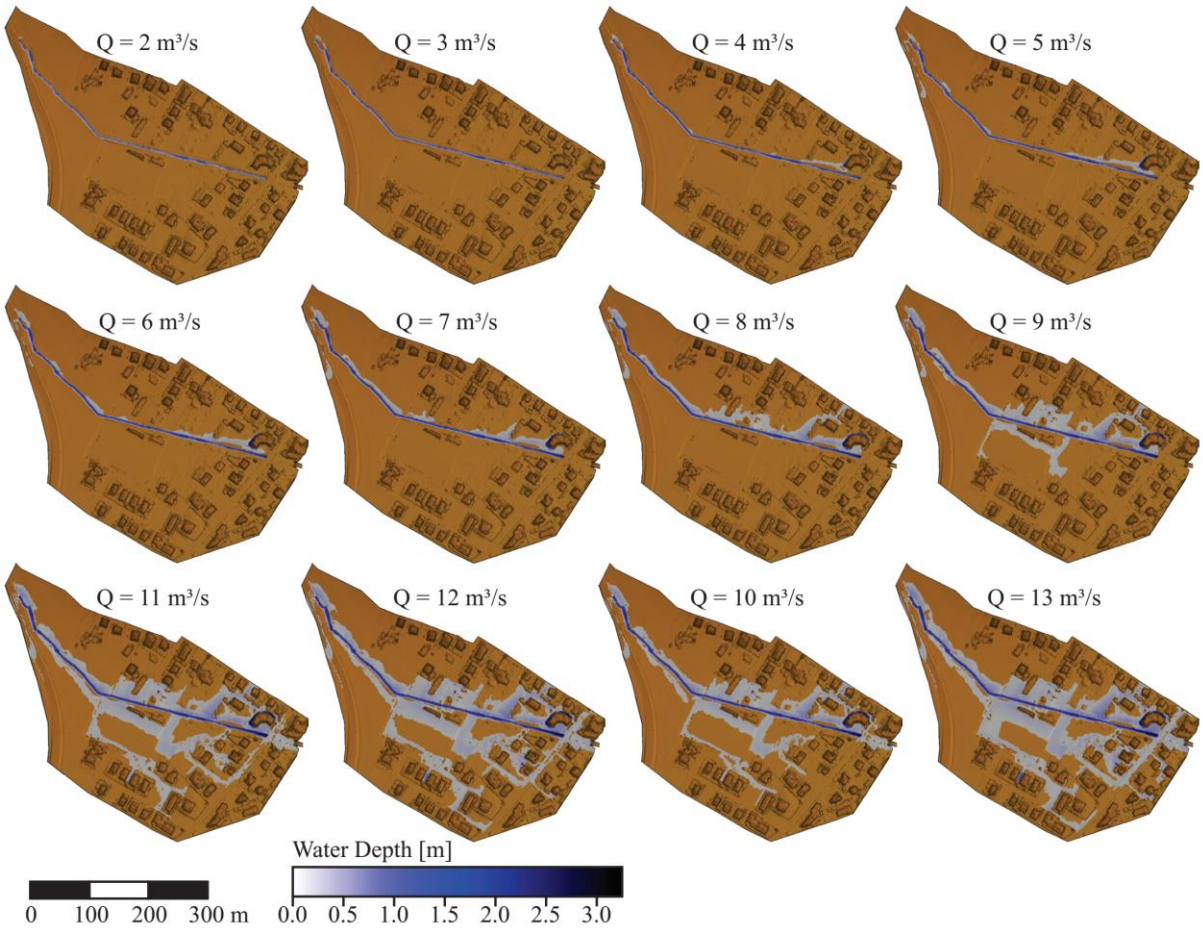

Figure 11. Overview of the resulting floods with progressive values of the maximum flow

Moreover, it was possible to numerically approximate the maximum value of the rainfall flow that the channel was able to drain, in the case of a correct maintenance, which is about 8 m^3/s. However, it was observed that flooding events could possibly reach greater values. By the means of the Guidelines provided by the Department of the Interior Bureau of Reclamation of Colorado, USA, the risk map for adults was also calculated. The map also shows an increasing risk in the proximity of a small bridge located in the examined area. In conclusion, this work highlights the importance of the correct maintenance of rainwater drainage canals, even on small scales, in order to significantly mitigate the inherent hydrogeological risk. It also tries to promote a conscious management and a knowledgeable future planning of anthropic activities, assisted by accurate numerical simulations of phenomena.

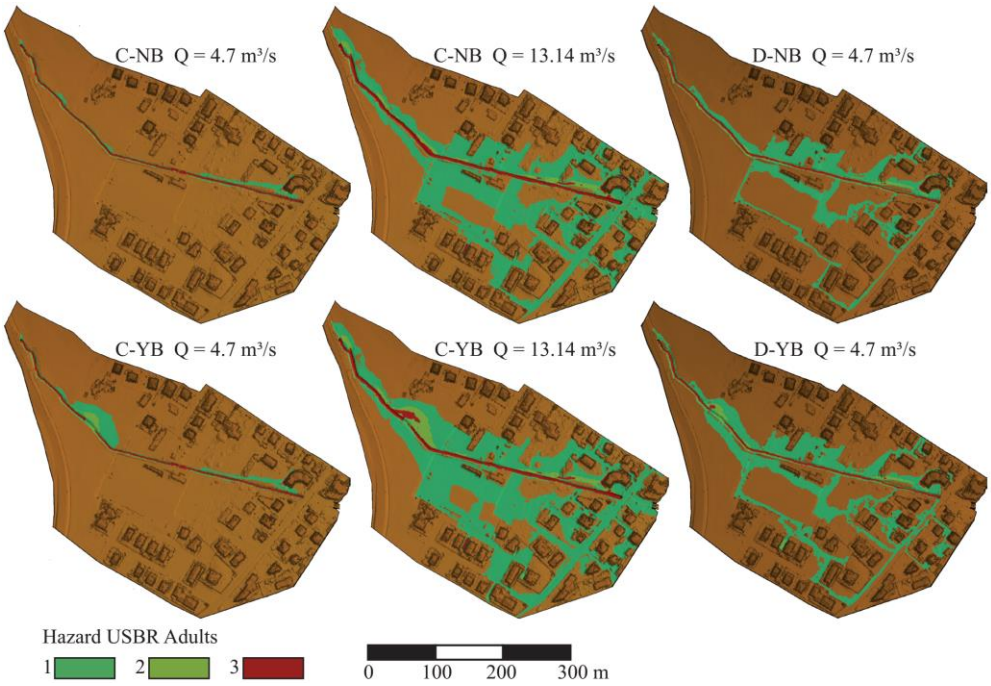

Figure 12. Estimated risk maps for adult individuals as described by [23]

References

[1] A. Pasculli. CFD-FEM 2D Modelling of a local water flow. Some numerical results. *Alpine and Mediterranean Quaternary*, 21(B), (1), 215-228; ISSN: 22797327; SCOPUS: 2-s2.0-84983037047, 2008.

[2] A. Pasculli and N. Sciarra. A probabilistic approach to determine the local erosion of a watery debris flow. *XI IAEG International Congress*; Liege, Belgium, 3-8 September Paper S08-08; SCOPUS id: 2-s2.0-84902449614, 2006.

[3] A. Pasculli and L. Minatti. Dam break Smoothed Particle Hydrodynamic modeling based on Riemann solvers. *Advances in Fluid Mechanics VIII, WIT Transactions on Engineering Sciences*, WIT Press; DOI: 10.2495/AFM100131; SCOPUS id: 2-s2.0-78449235684, (6) 9, pp. 145-156., 2010.

[4] L. Minatti, A. Pasculli. SPH numerical approach in modelling 2D muddy debris flow. *5th International Conference on Debris-Flow Hazards Mitigation Mechanics, Prediction and Assessment* (Padua 15-17 June 2011) DOI: 10.4408/IJEGE.2011-03.B-052. Casa Editrice Università La Sapienza Roma; pp. 467-475; SCOPUS id: 2-s2.0-84861619060, 2011.

[5] A. Pasculli, L. Minatti, N. Sciarra, E. Paris. SPH modeling of fast muddy debris flow: Numerical and experimental comparison of certain commonly utilized approaches. *Italian Journal of Geosciences*, 132 (3), 350-365; doi: 10.3301/IJG.2013.01; SCOPUS id: 2-s2.0-84886468697, 2013.

[6] A. Pasculli, L. Minatti, N. Sciarra. Insights on the application of some current SPH approaches for the study of muddy debris flow: Numerical and experimental comparison. *Wit Transaction 10th International Conference on Advances in Fluid Mechanics, AFM 2014*; Coruna; Spain, 82, 3–14; doi: 10.2495/AFM140011; SCOPUS id: 2-s2.0-84907611231, 2014.

[7] M. Pastor, T. Blanc, B. Haddad, S. Petrone, M. Sanchez Morles, V. Drempetic, D. Issler, G.B. Crosta, L. Cascini, G. Sorbino, S. Cuomo. Application of a SPH depth-integrated model to landslide run-out analysis. *Landslides* 11, 793-812, 2014.

[8] A. Pasculli and C. Audisio. Cellular Automata Modelling of Fluvial Evolution: Real and Parametric Numerical Results Comparison Along River Pellice (NW Italy). *Environmental*

Modeling and Assessment 20, (5), 425-441; doi: 10.1007/s10666-015-9444-8; SCOPUS id: 2-s2.0-84940588890, 2015.

[9] C. Audisio, A. Pasculli, N. Sciarra. Conceptual and numerical models applied on the river pellice (North western italy). *Engineering Geology for Society and Territory* 3, 327-330; DOI: 10.1007/978-3-319-09054-2-68; SCOPUS id: 2-s2.0-84944586202, 2015.

[10] A. Pasculli, C. Audisio, G. Lollino. Application of cellular automaton model for river morphological studies: CAESAR and the Pellice River (Piedmont, Italy). *Rendiconti Online Società Geologica Italiana* 11 (1), 118-119; ISSN: 20358008; SCOPUS id: 2-s2.0-84863090597, 2010.

[11] A. Pasculli, C. Audisio, N. Sciarra. Water and sediment output evaluation using cellular automata on alpine catchment: Soana, Italy - Test case. *IOP Conference Series: Earth and Environmental Science* 95, 1-8; doi: 10.1088/1755-1315/95/2/022031; SCOPUS id=2-s2.0-85044335598, 2017.

[12] Hydronia LLC. RiverFlow2D, Two-Dimensional Flood and River Dynamics Model, Reference Manual, www.hydronia.com, 2017.

[13] M. Calista, E. Miccadei, A. Pasculli, T. Piacentini, M. Sciarra, N. Sciarra. Geomorphological features of the Montebello sul Sangro large landslide (Abruzzo, Central Italy). *Journal of Maps*, 12 (5), 882-891; DOI: 10.1080/17445647.2015.1095134; SCOPUS id: 2-s2.0-84944909158, 2016.

[14] A. Pasculli, J. Cinosi, L. Turconi, N. Sciarra. Parametric study of an Alpine wet debris flow event (Novalesa, Torino, Italy) applying the Finite Volume Method (FVM). Comparison with available experimental data. *IOP Conference Series: Earth and Environmental Science, Prague* 221, 1-11, doi: 10.1088/1755-1315/221/1/012160; SCOPUS id=2-s2.0-85063483941, 2019.

[15] L. Esposito, A.W. Esposito, A. Pasculli, N. Sciarra. Particular features of the physical and mechanical characteristics of certain Phlegraean pyroclastic soils. *CATENA* 104, 186-194; doi: 10.1016/j.catena.2012.11.009; SCOPUS id: 2-s2.0-84873130083, 2013.

[16] A. Pasculli, N. Sciarra, L. Esposito, A.W. Esposito. Effects of wetting and drying cycles on mechanical properties of pyroclastic soils. *CATENA* 156, 113-123; doi: 10.1016/j.catena.2017.04.004; SCOPUS id=2-s2.0-85017109027, 2017.

[17] C. Di Nucci, A. Russo Spena. On the steady two-dimensional open channel flow. *Journal of Interdisciplinary Mathematics*, 21 (3), 579–594, 2018.

[18] J. Murillo, P. Garcia-Navarro. Weak solutions for partial differential equations with source terms: application to the shallow water equations. *Journal of Computational Physics*, 229 (11), 4327-4368, 2010.

[19] C. Vreugdenhil. *Numerical methods for shallow water flow*. Water Science and Technology Library. Kluwer Academic Publishers, 1994, pp- 272.

[20] V.T. Chow. Open-channel hydraulics. New York, McGraw-Hill Book Company, pp. 680, 1959.

[21] USDA, United States Department of Agricolture. Urban Hydrology for Small Watersheds TR-55., 1986.

[22] J. Cinosi, A. Pasculli, N. Sciarra. Impact of territory Management on Urban Flood; a test case**.** Accepted for publication in *Italian Journal of Engineering Geology and Environment.* Special Issue 1 (2019) Sapienza Università Editrice Doi: 10-.4408/IjEGE.2019-01-S-XX.

[23] Downstream Hazard Classification Guidelines. Acer Technical Memorandum N° 11; Assistant Commissioner Engineering and Research Denver, Colorado USA, U.S. Department of the Interior Bureau of Reclamation, 1988; pp. 56.